Optimization of perovskite solar cell with MoS₂-based HTM layer using hybrid L₂₇ Taguchi-GRA based genetic algorithm

Khairil Ezwan Kaharudin[1,2], Fauziyah Salehuddin[1], Nabilah Ahmad Jalaludin[1], Anis Suhaila Mohd Zain[1], Faiz Arith[1], Siti Aisah Mat Junos[1], Ibrahim Ahmad[3]

[1]Micro and Nano Electronics (MiNE), Centre for Telecommunication Research and Innovation (CeTRI), Faculty of Electronics and Computer Technology and Engineering (FTKEK), Universiti Teknikal Malaysia Melaka (UTeM), Melaka, Malaysia
[2]Faculty of Engineering and Built Environment, Department of Electrical and Electronic Engineering, Lincoln University College (Main Campus), Petaling Jaya, Malaysia
[3]College of Engineering (CoE), Centre for Micro and Nano Engineering (CMNE), Universiti Tenaga Nasional (UNITEN), Kajang, Malaysia

Article Info

ABSTRACT

This article proposes an optimization method to predictively model the perovskite solar cell with molybdenum disulfide (MoS₂) based inorganic hole transport material (HTM) for improved fill factor (FF) and power conversion efficiency (PCE) by finding the most optimum thickness and donor/acceptor concentration for each layer via a hybrid L_{27} Taguchi grey relational analysis (GRA) based genetic algorithm (GA). Numerical simulation of the device is carried out by employing one-dimensional solar cell capacitance simulator (SCAPS-1D) while the optimization procedures are developed based on combination of multiple methods; L_{27} Taguchi orthogonal array, GRA, multiple linear regression (MLR), and GA. The results of post-optimization reveal that the most optimum layer parameters for improved FF and PCE are predicted as follows; SnO_2F thickness (0.855 μm), SnO_2F donor concentration (9.206×10^{18} cm⁻³), TiO_2 thickness (0.011 μm), TiO_2 donor concentration (9.306×10^{16} cm⁻³), $CH_3NH_3PbI_3$ thickness (0.897 μm), $CH_3NH_3PbI_3$ donor concentration (0.906×10^{13} cm⁻³), MoS_2 thickness (0.154 μm), and MoS_2 acceptor concentration (9.373×10^{17} cm⁻³). Both FF and PCE of the device are improved by ~1.1% and ~12.6% compared to the pre-optimization.

Corresponding Author:

Fauziyah Salehuddin
Micro and Nano Electronics (MiNE), Centre for Telecommunication Research and Innovation (CeTRI)
Faculty of Electronics and Computer Technology and Engineering (FTKEK)
Universiti Teknikal Malaysia Melaka (UTeM)
Hang Tuah Jaya, Durian Tunggal, 76100 Melaka, Malaysia
Email: fauziyah@utem.edu.my

1. INTRODUCTION

In recent years, perovskite materials have been intensively investigated owing to their distinctive capacity to accommodate large-sized cations, which makes them extremely appropriate for the production of organic-inorganic solar cells. In addition to high yielding solution based production, perovskite solar cells have the same adaptability, portability, and cost effectiveness as dye-sensitized and organic solar cells [1]–[3]. In the preceding twelve years, substantial academic and industry researches have been conducted on the development and enhancement of perovskite solar cells. From 2010 to 2022, the power conversion efficiency (PCE) per device increased from 3.8% to beyond 30%, comparable with silicon-based solar cells [4]–[8]. Sufficient band gap, a significant absorption coefficient, longer diffusion lengths,

extraordinary charge mobility, and a decreased exciton recombination rate are exemplary optoelectronic characteristics that make perovskite solar cells particularly appealing [9]. Despite these remarkable features, there are still restrictions regarding stability, environmental protection, and PCE for their commercial application.

There have been several published research and applications on two-dimensional (2D) semiconductor materials due to their viability as platforms for ultra-fast carrier propagation. Molybdenum disulfide (MoS_2), molybdenum diselenide ($MoSe_2$), tungsten disulfide (WS_2), and tungsten diselenide (WSe_2) are all widely used 2D semiconducting materials primarily composed of a few thin sheets [10]–[13]. They were identified as crucial for their ultrafast transmission and accessibility of semiconducting band gaps. Materials like MoS_2 and $MoSe_2$ were developed specifically to remove generated holes from perovskite layers [14]–[18]. The observed high charge recombination is the greatest obstacle to achieving high efficiency utilizing these inorganic hole transport material (HTM), as do the methods documented for producing single sheets and few-layer MoS_2 (or Se_2) [19]–[22]. Due to the fact that the documented methods for producing single sheets and few-layer MoS_2 (or Se_2) do not provide uniform distribution of the medium, attaining high charge recombination is the crucial step towards achieving high efficiency with these inorganic HTMs [23]. Herein, it would be conceivable to generate high-efficiency, long-lasting, low-cost perovskite solar cells by using uniform, single-sheet MoS_2 (or Se_2) [24]–[28].

In both academia and industry, intrinsic variations in semiconductor materials have been extensively explored and studied. A recent investigation on the performance characteristics of a MoS_2 solar cell with antimony trisulfide (Sb_2S_3) HTM was carried out by Haque *et al.* [29] utilizing the one dimension solar capacitance simulator software tool (SCAPS-1D). The findings of the study showed that the values of J_{sc}, fill factor (FF), and PCE grow with an increase in the thickness of MoS_2, but the value of V_{oc} rises with a reduction in the absorber thickness for structures including an HTM layer. In addition, the V_{oc}, FF, and PCE were noticeably improved as a result of an increase in the doping density of the MoS_2 layer with HTM layer from 10^{14} to 10^{21} cm^{-3}. The impact of CdTe film thickness variation, the influence of CdTe defect density, and the effect of acceptor density on the MoS_2 layer was investigated, as reported by Singh *et al.* [30]. When compared to the fundamental CdTe structure, which did not have a MoS_2 layer anywhere in it, the efficiency of the solar cell is increased by 4.8% as a result of determining the optimal values for thickness, defect density, and acceptor density. Further, Kohnehpoushi *et al.* [31] have shown that if the MoS_2 thickness is made a little bit thicker, the J_{sc} of the perovskite device drops dramatically to 20.75 mA/cm^2. This implies that the thicker MoS_2 multilayers have a higher resistance and lower MoS_2 transmission.

For past few years, numerous optimization techniques have been utilized to identify the optimal combination of material parameters for solar cells that delivers the optimum electrical and optical performance. Response surface methodology (RSM) was employed in the design and optimization of nanocrystalline optically transparent coatings for Si solar cells, resulting in less than 5% reflection values over a broad range of wavelengths and near zero reflection at 560 nm for a 38 nm ZnO nanoparticle size, which can significantly improve photoactivity [32]. Optimization of an organic tandem solar cell using RSM has led to a 47.7% improvement in PCE as a result of changes in the thicknesses of the front and back cells [33]. In addition, the Taguchi technique was used to determine the ideal combination of bandgap for the front, rear, minimum, and along the x-axis of the CIGS solar cell, which optimally improves J_{sc}, V_{oc}, and FF, achieving an average efficiency of 22.08% [34]. Taguchi technique was also utilized to build photoanodes for dye-sensitized solar cells (DSSC), which showed a dramatic increase in FF and PCE [35]. The implementation of the Taguchi technique towards the prediction of the optimal thickness of cadmium sulfide (CdS), perovskite ($CH_3NH_3PbI_3$), and copper telluride (CuTe) resulted in higher levels of J_{sc}, V_{oc}, and PCE [36].

A limitation of optimizing solar cell structures through SCAPS-1D simulation without a design of experiment (DOE) approach is the risk of not fully exploring the parameter space. SCAPS-1D enables simulation of various solar cell parameters, including PCE, J-V characteristics, and quantum efficiency. However, without a systematic DOE, the optimization process might overlook parameter interactions or fail to reach the true global optimum, leading to less accurate performance predictions and a weaker understanding of how different factors impact the PSC's efficiency and stability. The effectiveness of PSCs is greatly influenced by the materials and fabrication methods used. The HTM layer is particularly important for charge transport and overall device efficiency. Traditional HTM materials have drawbacks such as high cost, instability, and complicated fabrication processes. MoS_2 is a promising alternative due to its excellent electrical properties, affordability, and stability. However, optimizing multiple layers along with MoS_2-based HTM layer for maximum PCE in PSCs requires a systematic approach.

In an effort to discover the ideal solution for improved solar cell performance, device simulation can be combined with numerous optimization techniques [37]–[42]. Before enduring real testing and production processes, these methodologies give predictive insight into the device's performance, saving a substantial amount of time and money [39]. In this study, a SCAPS-1D simulation incorporated with a hybrid

optimization approach consisting of L_{27} Taguchi orthogonal array, grey relational analysis (GRA), multiple linear regression (MLR), and genetic algorithm (GA) is proposed to optimize the layer parameters of the perovskite solar cell with MoS_2-based inorganic HTM for enhanced FF and PCE. The following contributes significantly to the optimization approach for perovskite solar cells using MoS_2-based inorganic HTM:
− To develop a new hybrid optimization approach consisting of L_{27} Taguchi orthogonal array, GRA, MLR, and GA.
− To identify the most significant layer parameters affecting the FF and PCE of the device.
− To predict the best combination of layer parameters that yields the highest possible FF and PCE of the device.
− To validate the proposed hybrid optimization approach by comparing it with pre-optimization and Taguchi-GRA technique.

2. METHOD

This current work comprises two main parts of methodology named as numerical simulation and hybrid optimization. The numerical simulation of the perovskite solar cell with MoS_2-based inorganic HTM is firstly performed by utilizing SCAPS-1D, an open source 1D simulation tool designed by the Department of Electronics and Information Systems, University of Gent, Belgium [43]. Afterwards, the proposed hybrid optimization method [44], [45] are conducted to further optimize multiple layer parameters of the device in an effort to attain better FF and PCE. Comprehensive description on both numerical simulation and hybrid optimization will be extensively elaborated in the following sub-sections.

2.1. Numerical simulation

The perovskite solar cell with MoS_2-based inorganic HTM (depicted in Figure 1) was numerically modeled by employing SCAPS-1D where the mathematical computation involved hole/electron continuity and poisson equations. Figure 2 depicts the energy band diagram of a perovskite solar cell with MoS_2-based Inorganic HTM. The initial layer parameters (listed in Table 1) including thickness and donor/acceptor concentration were taken from related previous experimental and theoretical data [31].
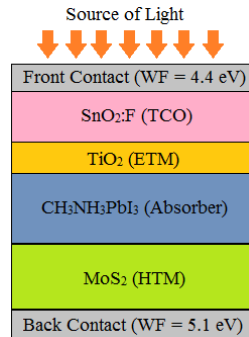

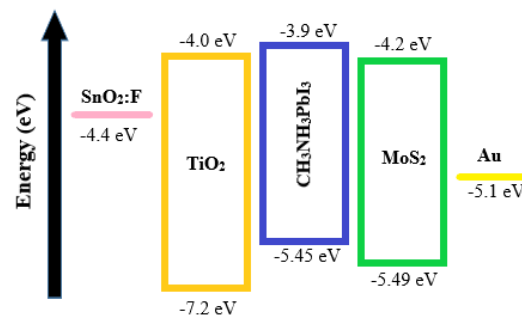Figure 1. Physical layout of perovskite solar cell with MoS_2-based inorganic HTM

Figure 2. Energy band diagram alignment

Table 1. Simulation parameters for multiple layers of materials

Parameters	SnO$_2$: F (TCO)	TiO$_2$ (ETM)	CH$_3$NH$_3$PbI$_3$ (absorber)	MoS$_2$ (HTM)
Thickness (μm)	0.2	0.04	0.4	0.3
χ (eV)	4	4	3.9	4.2
ε_r	9	100	6.5	3
E_g (eV)	3.5	3.2	1.55	1.29
μ_n (cm^2/Vs)	20	6×10^{-3}	2	100
μ_p (cm^2/Vs)	10	6×10^{-3}	2	150
N_v (cm^{-3})	1.8×10^{19}	1×10^{19}	1.8×10^{19}	1.8×10^{19}
N_c (cm^{-3})	2.2×10^{18}	1×10^{19}	2.2×10^{18}	2.2×10^{18}
N_a (cm^{-3})	-	-	-	1×10^{17}
N_d (cm^{-3})	1×10^{18}	1×10^{16}	$1x10^{13}$	-
N_t (cm^{-3})	1×10^{15}	1×10^{15}	2.5×10^{13}	$1x10^{14}$
Ref.	[46], [47]	[29], [48]	[31], [49]	[50]

In Table 1, the symbols; N_t, N_d, N_a, N_c, N_v, μ_p, μ_n, E_g, $\mathcal{E}_r$, and χ represent defect density, donor concentration, acceptor concentration, effective conduction band density, effective valence band density, hole mobility, electron mobility, bangap energy, relative permittivity, and electron affinity accordingly. To perform the simulation, the standard solar spectrum AM 1.5 was utilized as an optical energy source beamed at the front contact. The simulation solved carrier transport, drift-diffusion and recombination model to generate current density-voltage curves as the open circuit voltage (V_{oc}), short circuit current density (J_{sc}), FF and PCE were extracted and computed. The multiple layers of the device were virtually arranged in which the spray pyrolyzed fluorine-doped tin oxide (SnO_2F), titanium dioxide (TiO_2), perovskite ($CH_3NH_3PbI_3$), and MoS_2 were stacked together as transparent conducting oxide (TCO), electron transport material (ETM), absorber, and HTM layers accordingly. Both metal workfunctions for front and back contacts of the cell were fixed at 4.4 eV and 5.1 eV respectively.

2.2. Hybrid optimization

This section provides a comprehensive description on the hybrid optimization method comprising DoE based on L_{27} Taguchi orthogonal array, GRA, MLR, and GA. The proposed work-flow of the hybrid optimization method are depicted in Figure 3. After running 27 simulation runs based on the L_{27} Taguchi orthogonal array, the output properties of the device; FF and PCE were measured by using (1) and (2):

$$FF = \frac{V_{mp}J_{mp}}{V_{oc}J_{sc}} \tag{1}$$

$$PCE = \frac{J_{sc} \times FF \times V_{oc}}{P_{in}} \tag{2}$$

where V_{mp} and J_{mp} are voltage and current density at maximum power point respectively.
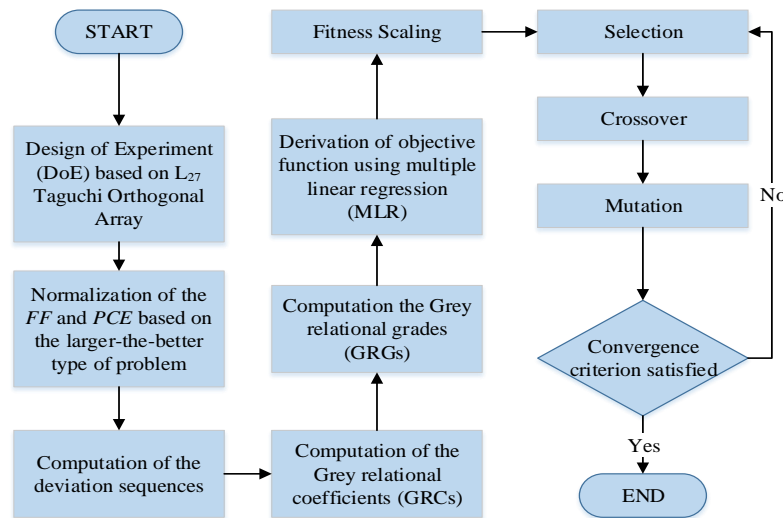

Figure 3. Proposed work-flow of the hybrid optimization method

The objective function was fed into a mechanism governed by GA where the initial population were occupied with initial magnitude of layer parameters. Basically, GA was utilized as a mechanism to search the local optimal magnitude of the objective function [51]–[56]. Although a linear objective function can typically be optimized by maximizing positive factors and minimizing negative ones, metaheuristics like GA may still be needed if the linear function involves complex constraints, particularly non-linear or combinatorial ones. Traditional optimization techniques may have difficulty handling such cases, but GA can navigate these constraints effectively by exploring a broader solution space. Additionally, in multi-objective scenarios, GA can provide a range of optimal solutions rather than just one, helping to balance competing objectives. The objective function was appropriately scaled to fit into the working space within specific range limited by the lower and upper boundaries which was later named as the fitness function (f_i). Since the main aim of this work was to search the local maxima of the function, the f_i was then inverted and numerically formulated as:

Minimize - $f(A, B, C, D, E, F, G, H)$
Subject to the constraints:
$0.1\ \mu m \leq A \leq 0.9\ \mu m$
$0.5 \times 10^{18}\ cm^{-3} \leq B \leq 9.5 \times 10^{18}\ cm^{-3}$
$0.01\ \mu m \leq C \leq 0.09\ \mu m$
$0.5 \times 10^{16}\ cm^{-3} \leq D \leq 9.5 \times 10^{16}\ cm^{-3}$
$0.1\ \mu m \leq E \leq 0.9\ \mu m$
$0.5 \times 10^{13}\ cm^{-3} \leq F \leq 9.5 \times 10^{13}\ cm^{-3}$
$0.1\ \mu m \leq G \leq 0.9\ \mu m$
$0.5 \times 10^{17}\ cm^{-3} \leq H \leq 9.5 \times 10^{17}\ cm^{-3}$

Through iteration of selection, crossover and mutation, the most local maxima point of the f_i should be identified. For random numbers of iteration, those processes were halted mainly due to no further increase exhibited in the fitness curve. At this stage, the maximum magnitude of the f_i were identified whereby the new population; SnO$_2$F thickness, SnO$_2$F donor concentration, TiO$_2$ thickness, TiO$_2$ donor concentration, CH$_3$NH$_3$PbI$_3$ thickness, CH$_3$NH$_3$PbI$_3$ donor concentration, MoS$_2$ thickness and MoS$_2$ acceptor concentration should be successfully predicted. For selection, the roulette wheel method is employed, single-point is used for crossover, and uniform random is the mutation method. The initial preferences for the GA optimization were shown as:

Type=real-valued
Population size=50
Number of generations=1,000
Elitism=2
Crossover probability=0.8
Mutation probability=0.1

3. RESULT AND DISCUSSION

This section provides a comprehensive discussion on the results of the predictive analytics. The data retrieved after being processed via both L$_{27}$ Taguchi orthogonal array and GRA are recorded in Table 2. The respective magnitudes of deviation sequences, GRCs and GRGs for 27 experimental rows are calculated accordingly using the appropriate equations aforementioned in previous section.

Table 2. Deviation sequences, GRCs, GRGs, and ranks

Exp. no.	Deviation sequences, Δ_{oi} (n)		GRC (n)		GRG (n)	Rank
	FF	PCE	FF	PCE		
1	0.938931	0.928349	0.34748	0.350055	0.348767	26
2	0.274809	0.239875	0.64532	0.675789	0.660555	11
3	0.328244	0	0.603687	1	0.801843	4
4	0.236641	0.725857	0.678756	0.407878	0.543317	19
5	0.053435	0.17757	0.903448	0.737931	0.82069	2
6	0.526718	0.227414	0.486989	0.687366	0.587178	17
7	0.068702	0.672897	0.879195	0.426295	0.652745	13
8	0.51145	0.439252	0.49434	0.532338	0.513339	22
9	0.244275	0.383178	0.671795	0.566138	0.618966	14
10	0.877863	0.962617	0.362881	0.341853	0.352367	25
11	0.221374	0.277259	0.693122	0.643287	0.668204	10
12	0.290076	0.034268	0.63285	0.93586	0.784355	5
13	0.358779	0.772586	0.582222	0.392901	0.487562	24
14	0.167939	0.227414	0.748571	0.687366	0.717969	7
15	0.671756	0.274143	0.42671	0.645875	0.536293	21
16	0	0.654206	1	0.433198	0.716599	8
17	0.427481	0.423676	0.539095	0.541315	0.540205	20
18	0.183206	0.05296	0.731844	0.904225	0.818034	3
19	1	1	0.333333	0.333333	0.333333	27
20	0.366412	0.317757	0.577093	0.611429	0.594261	16
21	0.419847	0.074766	0.543568	0.869919	0.706744	9
22	0.160305	0.738318	0.757225	0.403774	0.5805	18
23	0	0.193146	1	0.721348	0.860674	1
24	0.473282	0.239875	0.513725	0.675789	0.594757	15
25	0.061069	0.688474	0.891156	0.420708	0.655932	12
26	0.526718	0.454829	0.486989	0.523654	0.505322	23
27	0.244275	0.087227	0.671795	0.851459	0.761627	6

The rank of each experimental row is determined based on the highest computed GRGs. The GRA results indicate that the experimental row no. 23 has the highest rank of GRG compared to others at 0.8607. This justifiably implies that the 23rd experimental row has the best combinational layer parameters yielding the optimal FF and PCE of the perovskite device. The computed GRGs for each row can be evenly distributed into the respective layer parameters, owing to the orthogonality of the DoE L$_{27}$ Taguchi orthogonal array. Therefore, the GRGs for each individual layer parameters with their corresponding levels are computed and summarized in Table 3. From Table 3, the optimal levels of layer parameters representing the highest GRG are; SnO$_2$F thickness (0.4 μm), SnO$_2$F donor concentration (9×10^{18} cm^{-3}), TiO$_2$ thickness (0.04 μm), TiO$_2$ donor concentration (5×10^{16} cm^{-3}), CH$_3$NH$_3$PbI$_3$ thickness (0.8 μm), CH$_3$NH$_3$PbI$_3$ donor concentration (1x10^{13} cm^{-3}), MoS$_2$ thickness (0.4 μm) and MoS$_2$ acceptor concentration (9×10^{17} cm^{-3}). Based on the information in Table 3, the analysis of variance (ANOVA) is carried out to determine the significance of each layer parameters on influencing the GRG variation. The ANOVA results for this work are summarized in Table 4.

Table 3. GRG for layer parameters at multiple levels

Symbol	Layer parameters	GRG		
		Low	Medium	High
A	SnO$_2$:F thickness	0.6164	0.6246	0.6215
B	SnO$_2$:F donor concentration	0.5834	0.6365	0.6425
C	TiO$_2$ thickness	0.6580	0.6310	0.5735
D	TiO$_2$ donor concentration	0.6084	0.6289	0.6251
E	CH$_3$NH$_3$PbI$_3$ thickness	0.5147	0.6535	0.6900
F	CH$_3$NH$_3$PbI$_3$ donor concentration	0.6271	0.6124	0.6116
G	MoS$_2$ thickness	0.6149	0.6337	0.6139
H	MoS$_2$ acceptor concentration	0.4791	0.6370	0.7464

Table 4. ANOVA results

Layer parameter	DF	SSQ	MS	F-ratio	Contribution (%)
A	2	0.000108	5.38111E-05	0.268844	0.059545
B	2	0.006365	0.003182509	15.90008	3.521612
C	2	0.011187	0.005593413	27.94515	6.189402
D	2	0.000717	0.000358317	1.790183	0.396497
E	2	0.051286	0.025643129	128.1152	28.37546
F	2	0.000547	0.00027372	1.367528	0.302885
G	2	0.000749	0.000374308	1.870075	0.414192
H	2	0.108382	0.054191056	270.743	59.96522
Error	7	0.001401	0.000200157	-	0.775194
Total	23	0.180742	0.089870421	-	100

In addition, the percentage contribution of layer parameters on the GRG are displayed in Figure 4. It is clearly shown that the most significant layer parameters influencing GRG variation are layer parameter H (MoS$_2$ acceptor concentration) with ~60% of contribution, followed by layer parameter E (CH$_3$NH$_3$PbI$_3$ thickness) with ~28% of contribution. The remaining layer parameters can be considered neutral mainly due to their extremely small percentage contribution as they would not inflict any significant alteration on the GRG. The correlation between eight layer parameters and the GRGs are further analyzed using MLR method in which normal Q-Q plot is extracted as depicted in Figure 5. The retrieved data are plotted against a theoretical normal distribution in which the data points should form an approximate straight line. Spreading away from this straight line indicate the data points are spreading away from normality.

Using MLR method, the objective function of those correlation can be derived in which the regression coefficients for each layer parameters are estimated as (3):

$$Y = 0.28341 + 0.012708 * A + 0.007394 * B - 2.113125 * C + 0.002084 * D + 0.42741 * E - 0.001939 * F - 0.005313 * G + 0.033417 * H \qquad (3)$$

However, the objective function needs to be converted to the fitness function (f$_i$) where it is inverted and fitted within specified lower and upper boundaries for determining the local maxima of the curve. Thus, the f_i of the maximization problem can be formulated as (4):

$$fi = -0.28341 - 0.012708 * A - 0.007394 * B + 2.113125 * C - 0.002084 * D - 0.42741 * E + 0.001939 * F + 0.005313 * G - 0.033417 * H \qquad (4)$$
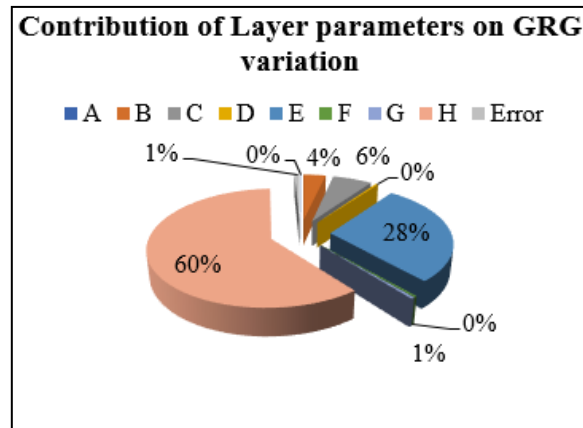
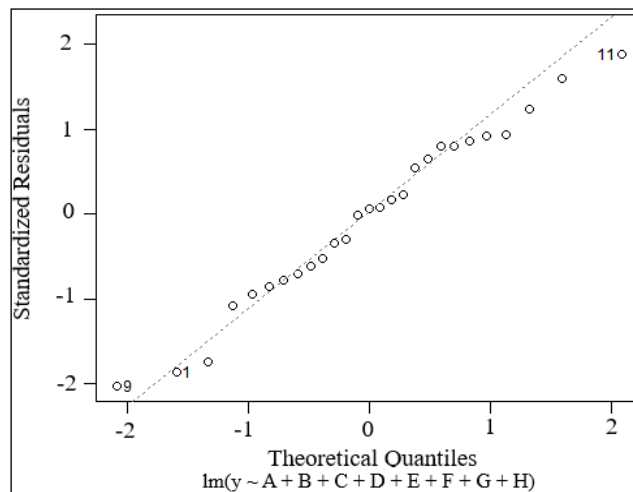Figure 4. Contribution of layer parameters on GRG variation

Figure 5. Normal Q-Q for multiple layer parameters

The f_i is repeatedly processed through the GA mechanisms; selection, crossover and mutation until no increase in fitness magnitude detected. For this work, the f_i has converged and instantly stopped at optimum magnitude after 1,000 cycles of generation as plotted in Figure 6. The maximum converged fitness magnitude of the GRG is observed to be 1.052030 associated with the predicted optimum layer parameters; SnO_2: F thickness (0.855 μm), SnO_2: F donor concentration (9.206×10^{18} cm^{-3}), TiO_2 thickness (0.011 μm), TiO_2 donor concentration (9.306×10^{16} cm^{-3}), $CH_3NH_3PbI_3$ thickness (0.897 μm), $CH_3NH_3PbI_3$ donor concentration (0.906×10^{13} cm^{-3}), MoS_2 thickness (0.154 μm), and MoS_2 acceptor concentration (9.373×10^{17} cm^{-3}). Lastly, the simulation of the perovskite solar cell is repeated using the predicted magnitude of layer parameters for verification. Figure 7 shows the comparison of the generated J-V transfer curves during pre-optimization, post-optimization via Taguchi-GRA and post-optimization via Taguchi-GRA-MLR-GA.

From the J-V transfer curves, the current density (J) of the device has been marginally improved by ~8.2% and ~8.7% during post-optimization using Taguchi-GRA and Taguchi-GRA-MLR-GA respectively. The magnitudes of current density during pre-analytics, post-analytics via GRA and post-optimization via Taguchi-GRA-MLR-GA are measured at 23.4 mA/cm^2, 25.51 mA/cm^2, and 25.63 mA/cm^2 respectively. The presence of MoS_2 as a HTM layer is one of the main factors improving the current density of device which predominantly due to higher level acceptor concentration. At lower doping concentration, the hole mobility is heavily influenced by scattering effects in the MoS_2 material itself. As temperature increases, the scattering effects becoming more dominant which subsequently result in lower hole mobility. By increasing the doping concentration of the MoS_2 material, the probability of the carriers colliding to each other will be high which cause significant improvement in hole mobility as well as total current density. Figure 8 depicts the

comparative cylindrical graph between FF and PCE of the device during pre-optimization, post-optimizarion using Taguchi-GRA and Taguchi-GRA-MLR-GA.
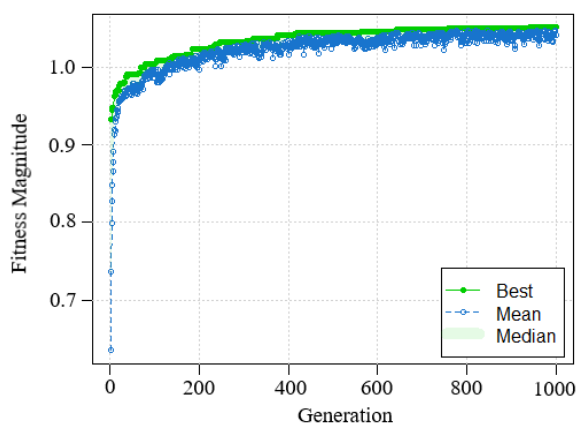

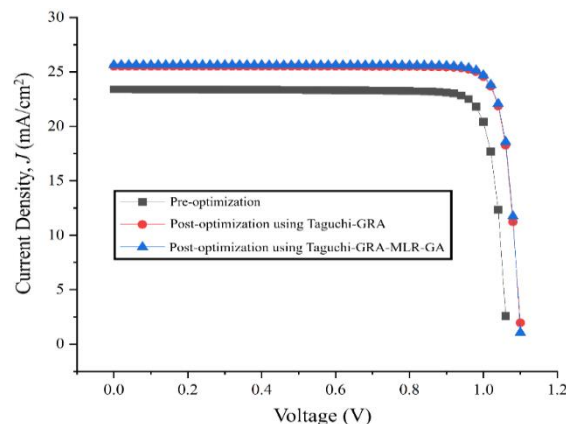Figure 6. Genetic algorithm performance during convergence

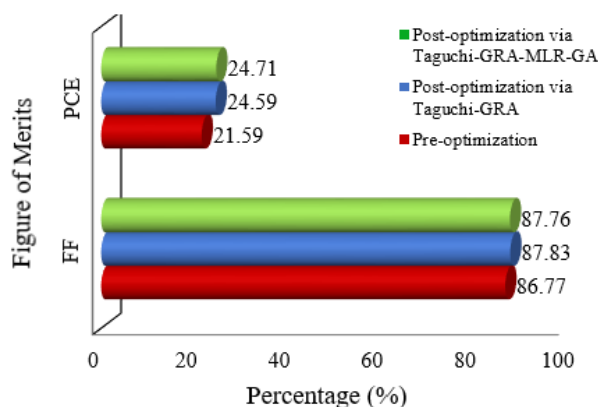Figure 7. J-V transfer curves during pre-optimization and post-optimization

Figure 8. Comparative cylindrical graph of FF and PCE during pre-optimization, post-optimization using Taguchi-GRA and Taguchi-GRA-MLR-GA

There is a marginal increase in PCE of the device during pre-optimization and post-optimization. The device has shown a slight improvement for approximately 12.2% and 12.6% via Taguchi-GRA and Taguchi-GRA-MLR-GA, respectively. In term of FF, improvement in percentage for both types of optimization method are almost indistinct where their corresponding *FF* has shown a slight improvement for approximately 1.2% and 1.1% via Taguchi-GRA and Taguchi-GRA-MLR-GA, respectively. Table 5 summarizes the overall results during pre-optimization, post-optimization using Taguchi-GRA and Taguchi-GRA-MLR-GA. Higher GRG implies that the opted layer parameters have contributed better multi-performance characteristics (FF and PCE) for the perovskite device. In this case, the GRG has been predictively improved by approximately 66.8% using Taguchi-GRA-MLR-GA optimization method. Besides that, the predicted GRG using Taguchi-GRA-MLR-GA are ~18.2% higher compared to Taguchi-GRA. This is solely due to the capability of the Taguchi-GRA-MLR-GA to further optimize the fitness function beyond the discrete magnitude of layer parameters. For instance, Taguchi-GRA alone is restricted to estimate only discrete magnitude of layer parameters while Taguchi-GRA-MLR-GA is capable of estimating continuous magnitude of layer parameters in which the lower and upper boundaries can be pre-specified according to desired preferences. Figure 9 shows the comparison of optimized FF and PCE with different algorithms.

Table 5. Overall results during pre-optimization, post-optimization using Taguchi-GRA and Taguchi-GRA-MLR-GA

Layer parameters	Pre-optimization	Post-optimization via Taguchi-GRA	Post-optimization via Taguchi-GRA-MLR-GA
SnO_2: F thickness	0.2 μm	0.4 μm	0.885 μm
SnO_2: F donor concentration	1×10^{18} cm^{-3}	9×10^{18} cm^{-3}	9.206×10^{18} cm^{-3}
TiO_2 thickness	0.04 μm	0.04 μm	0.011 μm
TiO_2 donor concentration	1×10^{16} cm^{-3}	5×10^{16} cm^{-3}	9.306×10^{16} cm^{-3}
$CH_3NH_3PbI_3$ thickness	0.4 μm	0.8 μm	0.897 μm
$CH_3NH_3PbI_3$ donor concentration	1×10^{13} cm^{-3}	1×10^{13} cm^{-3}	0.906×10^{13} cm^{-3}
MoS_2 thickness	0.3 μm	0.4 μm	0.154 μm
MoS_2 acceptor concentration	1×10^{17} cm^{-3}	9×10^{17} cm^{-3}	9.373×10^{17} cm^{-3}
FF	86.77%	87.83.%	87.77%
PCE	21.59%	24.59%	24.71%
Grey relational grade (GRG)	0.3488	0.8607	1.052
Improvement in the predicted GRG=~66.8%			

The utilization of Taguchi, GRA, and MLR extends to other algorithms besides GA. GA's optimization results are compared to those from pelican optimization algorithm (POA), marine predator algorithm (MPA), JAYA algorithm, and grey wolf optimizer (GWO) algorithm. The POA emulates the natural hunting behaviors and strategies of pelicans in which it simulate the hunting techniques and behaviors of pelicans [57]. The MPA optimizes efficiently by integrating the unique characteristics of Lévy strategy with Brownian motion features, proving superior in optimization tasks [58]. The JAYA algorithm effectively handles optimization tasks, both constrained and unconstrained, by moving solutions towards the best and avoiding the worst, all while maintaining simplicity [59]. The GWO algorithm replicates grey wolves' leadership and hunting techniques, utilizing alpha, beta, delta, and omega wolves to simulate their hierarchy and follow the hunting stages: searching, encircling, and attacking prey [60].
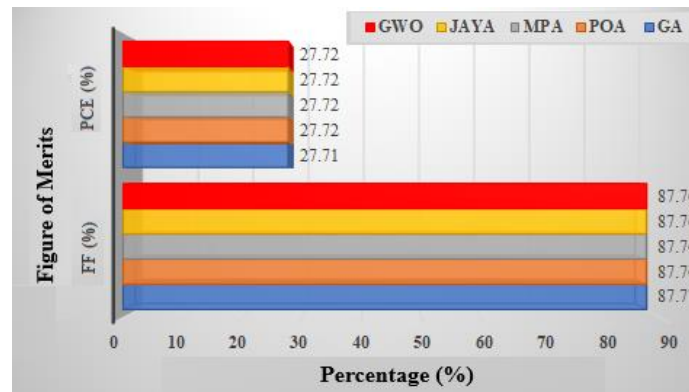
Figure 9. Comparison of optimized FF and PCE with different algorithms

The observed optimized FF and PCE are nearly indistinguishable, suggesting that all algorithms show comparable performance in this particular problem space. Thus, it can be concluded that the proposed hybrid optimization method is capable of predicting robust solutions that globally optimize the perovskite solar cell performances. In the future, metaheuristic algorithms and predictive learnings other than the GA could be empirically explored and integrated into the Taguchi DoE in an attempt to provide more precise and comprehensive results.

4. CONCLUSION

The perovskite solar cell with MoS_2-based inorganic HTM has been predictively modeled using a combination of SCAPS-1D, Taguchi GRA, MLR, and GA. The experimental data were mined using L_{27} Taguchi orthogonal array and subsequently analyzed using GRA. The magnitudes of FF and PCE were normalized and converted into a single representative unit based on higher-the better characteristic, called GRG. Based on ANOVA, the most significant layer parameters influencing GRG variation were MoS_2 acceptor concentration with ~60% of contribution, followed by $CH_3NH_3PbI_3$ thickness with ~28% of

contribution. MLR approach was then deployed to derive the objective function. With pre-specified lower and upper boundaries, the fitness function was determined and subsequently fed into GA mechanism in order to search the local maxima of the function. The most optimal fitness GRG magnitude was identified at 1.052 after 1,000 cycles of GA mechanism in which the optimum layer parameters were successfully predicted. Both FF and PCE of the perovskite device were slightly optimized by ~1.1% and ~12.6% respectively compared to the magnitudes during pre-optimization. The results clearly proved that the proposed hybrid optimization method was capable of predicting robust solutions that could globally optimize the perovskite solar cell performance. Future studies could explore and incorporate other metaheuristic algorithms and predictive learning approaches besides the GA within the Taguchi DoE to obtain more accurate and comprehensive results. These significant findings highlight the considerable progress achieved in modeling the PSC structure. Ultimately, this work's results can direct researchers in fabricating highly efficient PSCs in the future.

REFERENCES
[1] P. Liu et al., "Low-cost and Efficient Hole-Transport-Material-free perovskite solar cells employing controllable electron-transport layer based on P25 nanoparticles," Electrochimica Acta, vol. 213, pp. 83–88, Sep. 2016, doi: 10.1016/j.electacta.2016.07.095.

[2] H. J. Snaith, "Perovskites: The emergence of a new era for low-cost, high-efficiency solar cells," Journal of Physical Chemistry Letters, vol. 4, no. 21, pp. 3623–3630, Nov. 2013, doi: 10.1021/jz4020162.

[3] M. S. G. Hamed and G. T. Mola, "Mixed Halide Perovskite Solar Cells: Progress and Challenges," Critical Reviews in Solid State and Materials Sciences, vol. 45, no. 2, pp. 85–112, Mar. 2020, doi: 10.1080/10408436.2018.1549976.

[4] D. W. de Quilettes et al., "Impact of microstructure on local carrier lifetime in perovskite solar cells," Science Express, vol. 348, no. 6235, pp. 683-686, 2015, doi: 10.1126/science.aaa533.

[5] C. Wehrenfennig, G. E. Eperon, M. B. Johnston, H. J. Snaith, and L. M. Herz, "High charge carrier mobilities and lifetimes in organolead trihalide perovskites," Advanced Materials, vol. 26, no. 10, pp. 1584–1589, Mar. 2014, doi: 10.1002/adma.201305172.

[6] B. Roose, "Perovskite Solar Cells," Energies, vol. 15, no. 17, pp. 14–16, Sep. 2022, doi: 10.3390/en15176399.

[7] P. Roy, A. Ghosh, F. Barclay, A. Khare, and E. Cuce, "Perovskite Solar Cells: A Review of the Recent Advances," Coatings, vol. 12, no. 8, pp. 1–24, Jul. 2022, doi: 10.3390/coatings12081089.

[8] J. L. Prasanna et al., "Bandgap graded perovskite solar cell for above 30% efficiency," Optik, vol. 269, pp. 1–10, Nov. 2022, doi: 10.1016/j.ijleo.2022.169891.

[9] H. Liu et al., "Improvement Strategies for Stability and Efficiency of Perovskite Solar Cells," Nanomaterials, vol. 12, no. 19, pp. 1–18, 2022, doi: 10.3390/nano12193295.

[10] M. Alla et al., "Towards lead-free all-inorganic perovskite solar cell with theoretical efficiency approaching 23%," Materials Technology, vol. 37, no. 14, pp. 2963–2969, Dec. 2022, doi: 10.1080/10667857.2022.2091195.

[11] A. T. Ngoupo and J.-M. B. Ndjanka, "Performance enhancement of Sb2Se3-based solar cell with hybrid buffer layer and MoSe2 as a hole transport material using simulator device," Discover Mechanical Engineering, vol. 1, no. 5, pp. 1–18, Nov. 2022, doi: 10.1007/s44245-022-00005-0.

[12] M. A. Rahman, "Performance analysis of WSe2-based bifacial solar cells with different electron transport and hole transport materials by SCAPS-1D," Heliyon, vol. 8, no. 6, pp. 1–11, Jun. 2022, doi: 10.1016/j.heliyon.2022.e09800.

[13] X. He, Y. Iwamoto, T. Kaneko, and T. Kato, "Fabrication of near-invisible solar cell with monolayer WS2," Scientific Reports, vol. 12, no. 1, pp. 1–8, Jul. 2022, doi: 10.1038/s41598-022-15352-x.

[14] N. E. Safie, M. N. F. M. Sairi, M. A. Azam, and A. Takasaki, "Development and analysis of rGO-MoS2 nanocomposite as top electrode for the application of inverted planar perovskite solar cells via SCAPS-1D device simulation," Journal of Materials Research, vol. 37, no. 20, pp. 3372–3383, Oct. 2022, doi: 10.1557/s43578-022-00652-9.

[15] D. Soro et al., "Simulation of a CIGS Solar Cell with CIGSe2/MoSe2/Mo Rear Contact Using AFORS-HET Digital Simulation Software," Modeling and Numerical Simulation of Material Science, vol. 12, no. 2, pp. 13–23, 2022, doi: 10.4236/mnsms.2022.122002.

[16] P. N. A. Fahsyar, N. A. Ludin, N. F. Ramli, P. I. Zulaikha, S. Sepeai, and A. S. H. Md Yasir, "Stabilizing high-humidity perovskite solar cells with MoS2 hybrid HTL," Scientific Reports, vol. 13, no. 1, pp. 1–10, Jul. 2023, doi: 10.1038/s41598-023-39189-0.

[17] W. Qun, "The organic-inorganic solar cells device structure with different transport layers and compounds: The Guidelines for researchers," World Journal of Advanced Research and Reviews, vol. 17, no. 1, pp. 846–855, Jan. 2023, doi: 10.30574/wjarr.2023.17.1.0101.

[18] M. F. Wahid, U. Das, B. K. Paul, S. Paul, M. N. Howlader, and M. S. Rahman, "Numerical Simulation for Enhancing Performance of MoS2 Hetero-Junction Solar Cell Employing Cu2O as Hole Transport Layer," Materials Sciences and Applications, vol. 14, no. 09, pp. 458–472, 2023, doi: 10.4236/msa.2023.149030.

[19] M. Liang et al., "Improving stability of organometallic-halide perovskite solar cells using exfoliation two-dimensional molybdenum chalcogenides," npj 2D Materials and Applications, vol. 4, no. 1, pp. 1–8, Nov. 2020, doi: 10.1038/s41699-020-00173-1.

[20] A. Haseeb, H. Khan, and A. Basit, "Improving the Efficiency of lead-free non-toxic Rubidium Germanium Iodide Perovskite Solar Cell Using a Molybdenum Disulfide Interface Layer: A SCAPS 1D Simulation Study," International Research Journal of

Modernization in Engineering Technology and Science, no. 10, pp. 1801–1804, Oct. 2023, doi: 10.56726/irjmets45496.

[21] Mamta, R. Kumar, R. Kumari, K. K. Maurya, and V. N. Singh, "Sb2(S, Se)3-based photovoltaic cell with MoS2 as a hole transport layer: a numerical investigation," *Materials Today Sustainability*, vol. 20, Dec. 2022, doi: 10.1016/j.mtsust.2022.100218.

[22] A. K. Patel, R. Mishra, and S. K. Soni, "Performance enhancement of CIGS solar cell with two dimensional MoS2 hole transport layer," *Micro and Nanostructures*, vol. 165, May 2022, doi: 10.1016/j.micrna.2022.207195.

[23] P. N. A. Fahsyar *et al.*, "Correlation of simulation and experiment for perovskite solar cells with MoS2 hybrid-HTL structure," *Applied Physics A: Materials Science and Processing*, vol. 127, no. 5, pp. 1–10, May 2021, doi: 10.1007/s00339-021-04531-8.

[24] M. S. Islam and M. A. Haque, "Comparative Numerical Study of Hole Transport Layer to Improve the Performance of Cs2TiI6Based Perovskite Solar Cell," in *2021 5th International Conference on Electrical Information and Communication Technology, EICT 2021*, IEEE, Dec. 2021, pp. 1–5. doi: 10.1109/EICT54103.2021.9733656.

[25] A. D. Al-Ghiffari, N. A. Ludin, M. L. Davies, R. M. Yunus, and M. S. Suait, "Systematic review of molybdenum disulfide for solar cell applications: Properties, mechanism and application," *Materials Today Communications*, vol. 32, pp. 1–19, Aug. 2022, doi: 10.1016/j.mtcomm.2022.104078.

[26] S. Li, Y. L. Cao, W. H. Li, and Z. S. Bo, "A brief review of hole transporting materials commonly used in perovskite solar cells," *Rare Metals*, vol. 40, no. 10, pp. 2712–2729, 2021, doi: 10.1007/s12598-020-01691-z.

[27] W. Luo, J. Xu, and S. Liu, "Optimization of tin-based inverted perovskite solar cell with MoS2 interlayer by one-dimensional simulation," *Semiconductor Science and Technology*, vol. 38, no. 3, Mar. 2023, doi: 10.1088/1361-6641/acb16a.

[28] Y. Li *et al.*, "Improved efficiency of organic solar cell using MoS2 doped poly(3,4-ethylenedioxythiophene)(PEDOT) as hole transport layer," *Applied Surface Science*, vol. 590, Jul. 2022, doi: 10.1016/j.apsusc.2022.153042.

[29] M. D. Haque, M. H. Ali, M. F. Rahman, and A. Z. M. T. Islam, "Numerical analysis for the efficiency enhancement of MoS2 solar cell: A simulation approach by SCAP-1D," *Optical Materials*, vol. 131, pp. 1–10, Sep. 2022, doi: 10.1016/j.optmat.2022.112678.

[30] N. K. Singh, A. Agarwal, and T. Kanumuri, "Effect of MoS2 as a buffer layer on CdTe photovoltaic cell through numerical simulation," *Journal of Engineering Research (Kuwait)*, vol. 9, pp. 89–98, Aug. 2021, doi: 10.36909/jer.EMSME.13879.

[31] S. Kohnehpoushi, P. Nazari, and B. A. Nejand, "MoS2: a two-dimensional hole-transporting material for high-efficiency, low-cost perovskite solar cells," *Nanotechnology*, vol. 29, no. 20, pp. 1-8, 2018.

[32] Y. F. Makableh, H. Alzubi, and G. Tashtoush, "Design and optimization of the antireflective coating properties of silicon solar cells by using response surface methodology," *Coatings*, vol. 11, no. 6, pp. 1–13, Jun. 2021, doi: 10.3390/coatings11060721.

[33] A. R. Mohammed and I. S. Fahim, "Tandem Organic Solar Cell Optimization Using Response Surface Methodology," in *2020 International Conference on Data Analytics for Business and Industry: Way Towards a Sustainable Economy, ICDABI 2020*, IEEE, Oct. 2020, pp. 1–5. doi: 10.1109/ICDABI51230.2020.9325624.

[34] M. S. Bahrudin, Y. Yusoff, S. F. Abdullah, A. W. M. Zuhdi, N. Amin, and I. Ahmad, "A Parametric Optimization using Taguchi Method for Cu (In,Ga)(S,Se)2 Thin Film Solar Cell Device Simulation," *Journal of Energy and Environment*, vol. 12, no. 2, pp. 1–7, 2020.

[35] J. R. Zapata-Cruz, E. N. Armendáriz-Mireles, E. Rocha-Rangel, G. Suarez-Velazquez, D. González-Quijano, and W. J. Pech-Rodríguez, "Implementation of Taguchi method to investigate the effect of electrophoretic deposition parameters of SnO2 on dye sensitised solar cell performance," *Materials Technology*, vol. 34, no. 9, pp. 549–557, Jul. 2019, doi: 10.1080/10667857.2019.1591730.

[36] M. S. Bahrudin *et al.*, "Jsc and Voc optimization of perovskite solar cell with interface defect layer using taguchi method," in *IEEE International Conference on Semiconductor Electronics, Proceedings, ICSE*, pp. 192–196, 2018, doi: 10.1109/SMELEC.2018.8481203.

[37] B. R. Hunde and A. D. Woldeyohannes, "Performance analysis and optimization of perovskite solar cell using SCAPS-1D and genetic algorithm," *Materials Today Communications*, vol. 34, pp. 1–12, Mar. 2023, doi: 10.1016/j.mtcomm.2023.105420.

[38] A. G. Olabi *et al.*, "Optimal Parameter Identification of Perovskite Solar Cells Using Modified Bald Eagle Search Optimization Algorithm," *Energies*, vol. 16, no. 1, pp. 1–15, Jan. 2023, doi: 10.3390/en16010471.

[39] K. E. Kaharudin *et al.*, "Optimal modeling of perovskite solar cell with graphene oxide as hole transport layer using L32 (28) Taguchi design," *International Journal of Nanoelectronics and Materials*, vol. 17, no. 1, pp. 20–27, 2024, doi: 10.58915/ijneam.v17i1.448.

[40] K. E. Kaharudin, F. Salehuddin, A. S. M. Zain, and M. N. I. A. Aziz, "Application of taguchi-based grey fuzzy logic for simultaneous optimization in TiO2/WSix-based vertical double-gate MOSFET," *Journal of Telecommunication, Electronic and Computer Engineering*, vol. 9, no. 2–13, pp. 23–28, 2017.

[41] I. O. Oboh, U. H. Offor, and N. D. Okon, "Artificial neural network modeling for potential performance enhancement of a planar perovskite solar cell with a novel TiO$_2$/SnO$_2$ electron transport bilayer using nonlinear programming," *Energy Reports*, vol. 8, no. August, pp. 973–988, 2022, doi: 10.1016/j.egyr.2021.12.010.

[42] A. A. Abdelkadir, E. Oublal, M. Sahal, and A. Gibaud, "Numerical simulation and optimization of n-Al-ZnO/n-CdS/p-CZTSe/p-NiO (HTL)/Mo solar cell system using SCAPS-1D," *Results in Optics*, vol. 8, pp. 1–12, Aug. 2022, doi: 10.1016/j.rio.2022.100257.

[43] A. Niemegeers and M. Burgelman, "Numerical modelling of AC-characteristics of CdTe and CIS solar cells," *Conference Record of the Twenty Fifth IEEE Photovoltaic Specialists Conference - 1996*, Washington, DC, USA, 1996, pp. 901-904, doi: 10.1109/PVSC.1996.564274.

[44] K. E. Kaharudin *et al.*, "Predictive Analytics of Junctionless Double Gate Strained Mosfet Using Genetic Algorithm With Doe-Based Grey Relational Analysis," *Journal of Engineering Science and Technology*, vol. 18, no. 6, pp. 3077–3096, 2023.

[45] Z. Ziani, M. Y. Mahdad, M. Z. Bessenouci, M. C. Sekkal, and N. Ghellai, "Enhancing Multi-Junction Solar Cell Performance: Advanced Predictive Modeling and Cutting-Edge CIGS Integration Techniques," *Energies*, vol. 17, no. 18, pp. 0–25, 2024, doi: 10.3390/en17184669.

[46] M. K. Hossain *et al.*, "Combined DFT, SCAPS-1D, and wxAMPS frameworks for design optimization of efficient Cs2BiAgI6-based perovskite solar cells with different charge transport layers," *RSC Advances*, vol. 12, no. 54, pp. 34850–34873, 2022, doi: 10.1039/d2ra06734j.

[47] M. A. Salih, M. A. Mustafa, and B. A. A. Yousef, "Developing Lead-Free Perovskite-Based Solar Cells with Planar Structure in Confined Mode Arrangement Using SCAPS-1D," *Sustainability (Switzerland)*, vol. 15, no. 2, pp. 1–18, Jan. 2023, doi: 10.3390/su15021607.

[48] A. S. Shamsuddin, P. N. A. Fahsyar, N. A. Ludin, I. Burhan, and S. Mohamad, "Device simulation of perovskite solar cells with molybdenum disulfide as active buffer layer," *Bulletin of Electrical Engineering and Informatics*, vol. 8, no. 4, pp. 1251–1259,

Dec. 2019, doi: 10.11591/eei.v8i4.1596.

[49] Z. Liu *et al.*, "CH3NH3PbI3:MoS2 heterostructure for stable and efficient inverted perovskite solar cell," *Solar Energy*, vol. 195, pp. 436–445, Jan. 2020, doi: 10.1016/j.solener.2019.11.030.

[50] S. M. Seyed-Talebi, M. Mahmoudi, and C. H. Lee, "A Comprehensive Study of CsSnI3-Based Perovskite Solar Cells with Different Hole Transporting Layers and Back Contacts," *Micromachines*, vol. 14, no. 8, pp. 1–12, Aug. 2023, doi: 10.3390/mi14081562.

[51] A. S. Karaca *et al.*, "Optimization of synchrotron radiation parameters using swarm intelligence and evolutionary algorithms," *Journal of Synchrotron Radiation*, vol. 31, no. Pt 2, pp. 420–429, Mar. 2024, doi: 10.1107/S1600577524000717.

[52] M. Gao *et al.*, "The optimization method based on the coupling of genetic algorithm and ant colony algorithm for the exhaust outlet space arrangement," *AIP Advances*, vol. 14, no. 3, Mar. 2024, doi: 10.1063/5.0196294.

[53] D. T. Muhamediyeva, L. U. Safarova, and D. I. Umarov, "Application of a genetic algorithm in solving problems of environmental protection in agro-industrial production," *E3S Web of Conferences*, vol. 480, pp. 4–10, Jan. 2024, doi: 10.1051/e3sconf/202448003021.

[54] Z. A. Al-Sadi and D. J. Sadeq, "Genetic Algorithm-Based Well Placement Optimization: A Review of Studies," *Iraqi Geological Journal*, vol. 56, no. 2, pp. 246–264, 2023, doi: 10.46717/igj.56.2F.16ms-2023-12-22.

[55] D. T. Hai, D. Van Manh, and N. M. Nhat, "Genetic Algorithm Application for Optimizing Traffic Signal Timing Reflecting Vehicle Emission Intensity," *Transport Problems*, vol. 17, no. 1, pp. 5–16, Mar. 2022, doi: 10.20858/tp.2022.17.1.01.

[56] J. M. García, C. A. Acosta, and M. J. Mesa, "Genetic algorithms for mathematical optimization," *Journal of Physics: Conference Series*, vol. 1448, no. 1, pp. 1–6, Jan. 2020, doi: 10.1088/1742-6596/1448/1/012020.

[57] P. Trojovský and M. Dehghani, "Pelican Optimization Algorithm: A Novel Nature-Inspired Algorithm for Engineering Applications," *Sensors*, vol. 22, no. 3, pp. 1–34, Jan. 2022, doi: 10.3390/s22030855.

[58] A. Faramarzi, M. Heidarinejad, S. Mirjalili, and A. H. Gandomi, "Marine Predators Algorithm: A nature-inspired metaheuristic," *Expert Systems with Applications*, vol. 152, pp. 1–28, Aug. 2020, doi: 10.1016/j.eswa.2020.113377.

[59] R. V. Rao, "Jaya: A simple and new optimization algorithm for solving constrained and unconstrained optimization problems," *International Journal of Industrial Engineering Computations*, vol. 7, no. 1, pp. 19–34, 2016, doi: 10.5267/j.ijiec.2015.8.004.

[60] S. Mirjalili, S. M. Mirjalili, and A. Lewis, "Grey Wolf Optimizer," *Advances in Engineering Software*, vol. 69, pp. 46–61, Mar. 2014, doi: 10.1016/j.advengsoft.2013.12.007.

BIOGRAPHIES OF AUTHORS

Khairil Ezwan Kaharudin 🆔 📊 SC ➰ received Ph.D. in Electronic Engineering and M.Eng. degree in Computer Engineering from Technical University of Malaysia Melaka (UTeM), in 2017 and 2013 respectively. His Ph.D. project focused on the process optimization of vertical double gate MOSFET. His research's interests include computional microelectronics CMOS design, VLSI design, semiconductors, parameter variability, engineering optimization and artificial intelligence. Recently, his efforts emphasize on the simulation design of junctionless transistors, silicon-on-insulator (SOI) transistors, high-k/metal-gate stack technology, DoE, optimization methods, and computational intelligence. He can be contacted at email: khairilezwan@yahoo.com.my.

Fauziyah Salehuddin 🆔 📊 SC ➰ received the B.Sc. Degree in Electrical Engineering (Communication) from Universiti Teknologi Mara (UiTM), Malaysia in 2001 and the M.Sc. degree in Electrical, Electronic and System Engineering from Universiti Kebangsaan Malaysia, in 2003. She received the Ph.D. degree in Microelectronics Engineering from Universiti Tenaga Nasional (UNITEN), Malaysia in 2012. She joined Universiti Teknikal Malaysia Melaka (UTeM) in December 2001 as a tutor and is currently a Associate Professor at Faculty of Electronics and Computer Technology and Engineering (FTKEK), UTeM. Her research interest includes process and device simulation of nanoscale MOSFETs device, advanced CMOS design, optimization approach (DOE), and process parameter variability. She can be contacted at email: fauziyah@utem.edu.my.

Nabilah Ahmad Jalaludin 🆔 📊 SC ➰ received received the B.Eng. Degree in Electronic Engineering and M. Eng. Degree in Electronic Engineering (Electronic System) from Universiti Teknikal Malaysia Melaka (UTeM) in 2021 and 2022, respectively. She is currently pursuing a Ph.D. in Electronic Engineering at UTeM. Her research interests include device design, simulation of photovoltaic materials and devices, optimization, and predictive modelling. Recently, her work has focused on solar cell simulation design, DoE, and optimization approaches. She can be contacted at email: nabilahahmad98@gmail.com.

Anis Suhaila Mohd Zain received the B.Eng. degree in Electrical, Electronic, and System Engineering and M.Sc. degree in Microelectronics from Universiti Kebangsaan Malaysia (UKM), in 2000 and 2001 respectively. She received the Ph.D. degree in Electronics and Electrical Engineering from University of Glasgow (UK, Scotland), Malaysia in 2013. She joined Universiti Teknikal Malaysia Melaka (UTeM) in February 2002 as a lecturer and is currently a senior lecturer at the Faculty of Electronics and Computer Technology and Engineering (FTKEK), UTeM. Her research interest includes nanoscale device design and simulation, nanotechnology variability and reliability of emerging technology devices, and IC design for biomedical applications. She can be contacted at email: anissuhaila@utem.edu.my.

Faiz Arith received the B.Eng. in Electrical and Electronic Engineering from University of Fukui, Japan, in 2010. Then he obtained M.Sc. in Microelectronic from National University of Malaysia in 2012 and the Ph.D. degree in Semiconductor Devices from Newcastle University, United Kingdom, in 2018. Currently, he is Senior Lecturer and the Head of Micro and Nano Electronic Research Group in Universiti Teknikal Malaysia, Melaka, Malaysia. He is the author of two book chapters, more than 30 articles, and has won several innovation competitions. His main research interest is fabrication and simulation of semiconductor devices including solar cells, MOSFETs, power semiconductor devices and optoelectonic devices. He is a Technical Editor of the Journal of Telecommunication, Electronic and Computer Engineering, and has served as reviewer in more than 10 indexed reputable journals. He can be contacted at email: faiz.arith@utem.edu.my.

Siti Aisah Mat Junos received the B.Eng. degree in Electronic Engineering from Universiti Teknikal Malaysia (UTeM) in 2006 and the M.Sc. degree in Electrical, Electronic and System Engineering from Universiti Kebangsaan Malaysia (UKM), in 2009. She joined Universiti Teknikal Malaysia Melaka (UTeM) in September 2006 as a tutor and is currently a lecturer at Faculty of Electronics and Computer Technology and Engineering (FTKEK), UTeM. Her research interest is simulation of semiconductor devices including solar cells and nanoscale MOSFETs. She can be contacted at email: aisah@utem.edu.my.

Ibrahim Ahmad received the B.Sc. degree in Physics in 1980 from Universiti Kebangsaan Malaysia (UKM). He received the M.Sc. degree in Nuclear Science and Analytical Physics from UKM and University of Wales respectively, in year of 1991 and 1992. He received the Ph.D. degree in Electrical, Electronic and System Engineering from UKM in 2007. He joins the Department of Electrical, Electronic and System Engineering, UKM as a lecturer in 1997 to 2002, and as Associate Professor from 2002 to 2007. He involved in several management and technical positions with MINT, MIMOS and UKM. He is currently a Professor with the Department of Electronics and Communication Engineering, Universiti Tenaga Nasional, Malaysia. He is a senior member of the Institute of Electrical and Electronics Engineers (Senior MIEEE). He can be contacted at email: aibrahim@uniten.edu.my.